Statistical physics of grain-boundary engineering

E. S. McGarrity* and P. M. Duxbury†
Department of Physics and Astronomy, Michigan State University, East Lansing, Michigan 48823, USA

E. A. Holm‡
Materials and Process Modeling, Sandia National Laboratories, Albuquerque, New Mexico 87185-1411, USA
(Received 9 August 2004; published 4 February 2005)

Percolation theory is now standard in the analysis of polycrystalline materials where the grain boundaries can be divided into two distinct classes, namely "good" boundaries that have favorable properties and "bad" boundaries that seriously degrade the material performance. Grain-boundary engineering (GBE) strives to improve material behavior by engineering the volume fraction c and arrangement of good grain boundaries. Two key percolative processes in GBE materials are the onset of percolation of a strongly connected aggregate of grains, and the onset of a connected path of weak grain boundaries. Using realistic polycrystalline microstructures, we find that in two dimensions the threshold for strong aggregate percolation c_{SAP} and the threshold for weak boundary percolation c_{WBP} are equivalent and have the value $c_{\mathrm{SAP}}=c_{\mathrm{WBP}}=0.38(1)$, which is slightly higher than the threshhold found for regular hexagonal grain structures, $c_{RH}=2\sin(\pi/18)=0.347\ldots$. In three dimensions strong aggregate percolation and weak boundary percolation occur at different locations and we find $c_{\mathrm{SAP}}=0.12(3)$ and $c_{\mathrm{WBP}}=0.77(3)$. The critical current in high T_c materials and the cohesive energy in structural systems are related to the critical manifold problem in statistical physics. We develop a theory of critical manifolds in GBE materials, which has three distinct regimes: (i) low concentrations, where random manifold theory applies, (ii) critical concentrations where percolative scaling theory applies, and (iii) high concentrations, $c>c_{\mathrm{SAP}}$, where the theory of periodic elastic media applies. Regime (iii) is perhaps most important practically and is characterized by a critical length L_c, which is the size of cleavage regions on the critical manifold. In the limit of high contrast $\epsilon\to 0$, we find that in two dimensions $L_c\propto gc/(1-c)$, while in three dimensions $L_c\propto g\exp[b_0c/(1-c)]/[c(1-c)]^{1/2}$, where g is the average grain size, ϵ is the ratio of the bonding energy of the weak boundaries to that of the strong boundaries, and b_0 is a constant which is of order 1. Many of the properties of GBE materials can be related to L_c, which diverges algebraically on approach to $c=1$ in two dimensions, but diverges exponentially in that limit in three dimensions. We emphasize that GBE percolation processes and critical manifold behavior are very different in two dimensions as compared to three dimensions. For this reason, the use of two dimensional models to understand the behavior of bulk GBE materials can be misleading.

DOI: 10.1103/PhysRevE.71.026102 PACS number(s): 62.20.Mk, 05.10.−a

I. INTRODUCTION

There are many scientifically and technologically important materials where grain boundaries are critical to controlling material properties. Examples range from structural metallic and intermetallic materials [1–18] to polycrystalline high temperature superconductors [19–34] and ceramic varistors [35,36]. The grain boundaries in many of these materials can be separated into "good" boundaries and "bad" boundaries so that a network model with two types of network bond is appropriate. This is the general class of model which we consider in this contribution, where we define c to be the fraction of grain boundaries which are "good." We generate realistic polycrystalline microstructures using well established grain growth models [37–40] and we analyze percolation processes [24,25,32,34,41–46] and critical manifolds [20,21,25,47–50] in these grain structures using scaling ideas developed in statistical physics. Critical manifolds in polycrystalline microstructures are found using the maximum flow algorithm from computer science [51,52]. We present the results of large scale simulations for both two and three dimensional polycrystalline microstructures and we derive scaling laws which provide a very good description of the numerical data.

The optimization of critical currents in polycrystalline ceramic high temperature superconductors relies on low angle, high critical current, grain boundaries [19,26,29]. Typically grain boundaries between grains which are misoriented by less than about 5° have a critical current which is of order 100 times as large as that of high angle grain boundaries. Grain-boundary "maps" [26] or "networks" [18] of either special boundaries or "weak" boundaries have been experimentally determined and correlated with desired material properties [29]. One interesting property which we calculate is the critical current of a polycrystalline aggregate as a function of the fraction c of low angle grain boundaries. There are many papers discussing this quantity, with some focusing on the behavior near the percolation threshold c_{SAP} and on numerical simulations. Our previous studies [50,53,54] have presented the results of simulations of realistic bulk poly-

*Electronic address: mcgarrit@pa.msu.edu
†Electronic address: duxbury@pa.msu.edu
‡Electronic address: eaholm@sandia.gov

 ©2005 The American Physical Society

crystalline microstructures. A scaling theory for critical current in GBE materials based on the theory of periodic elastic media [55–57] leads to surprisingly good expressions for the critical current as a function of c in the high concentration regime, which is the regime of most practical interest. Several other properties of the critical manifold, such as its roughness, are also presented here and are also well described by the scaling theories which we derive.

An early success of grain-boundary engineering was the use of processing to increase the volume fraction of special grain boundaries in order to increase the corrosion resistance of Ni-16Cr-9Fe alloys [2,4–6,8,12]. In this application the onset of percolation of a path of weak grain boundaries is considered to be important, and we define the threshold for this percolation process to be c_{WBP}. We define the normalized penetration depth of weak boundaries l_P/L and calculate this quantity as a function of c. Creep and cracking processes have also been related to the grain-boundary character distribution [7,58]. The onset of a strong percolating aggregate is more relevant to these processes, and we define c_{SAP} as the threshold for this percolation process. We find the thresholds c_{SAP} and c_{WBP} for realistic polycrystalline microstructures.

A close connection exists between the statistical physics community and the fracture community in the area of fracture surface statistics. Following the suggestion by Mandlebrot [59] that fracture surfaces are fractal, there has been intense study of the physical origin of the roughness of fracture surfaces [60–62] and of relations between roughness and fracture toughness [63]. There is debate about whether the short distance roughness is described by quasistatic models of the sort described here, or by dynamical models [62]. Due to the ability to control the concentration c and grain size g in GBE materials, these systems present a tunable system in which to test their competing theories. The roughness simulations and scaling theory presented here provide a useful starting point in this discussion.

As well as defining c to be the fraction of "good" grain boundaries, we also use an "energy contrast ratio" ϵ which is the ratio of the grain-boundary energy to the grain interior energy. This energy contrast has different meanings in different applications. In the application to corrosion resistance it measures the susceptibility of high angle grain boundaries to permeation by corrosive agents, as compared to the bulk. In the case of high temperature superconductors it is the ratio of the critical current of high angle grain boundaries to that of low angle grain boundaries. In fracture applications it is the cohesive energy of poorly bonded boundaries as compared to well bonded boundaries. In magnetic applications it is the exchange constant of well isolated grains as compared to poorly isolated grains. The variable c also has different origins in different applications, for example in the case of high temperature superconductors it is the fraction of grain boundaries which have misorientation angles less than roughly 3%, while in the case of corrosion resistance it is the fraction of grain boundaries which are low order CSL boundaries. The percolation processes we study depend on the parameter c. The critical manifolds we discuss depend on both c and ϵ and are minimum energy interfaces in polycrystalline materials where a fraction c of the grain boundaries are assigned energy ϵ and the remaining grain boundaries as well as the grain interiors have energy 1.

The paper is organized as follows. In the next section, Sec. II, we discuss the numerical and theoretical methods we use to analyze percolation processes and critical manifolds in models of GBE materials. Section III presents data for the percolation processes which are relevant in GBE materials. Section IV presents data for the critical manifold (CM) and presents scaling theories for the behavior of the CM in various concentration regimes. The paper closes in Sec. V with a summary and discussion.

II. METHODS

In this section we briefly outline the computational tools and theoretical ideas used in the remainder of the paper.

A. Computational methods

We grow polycrystalline grain structures using a well tested Potts model algorithm [37–40]. Briefly, a q-state ferromagnetic Potts model on a hypercubic lattice is quenched from a high temperature state to zero temperature and a Monte Carlo procedure is used to anneal the Potts configuration of spins. Bonds between sites with different spin labels are considered to be grain boundaries. The typical grain size g increases with time as $t^{1/2}$. For the simulations described herein, we used 100 Potts labels in the three dimensional simulations and 256 Potts labels in the two dimensional simulations. The calculations are carried out on hypercubic lattices of size L^d sites, where d is the spatial dimension. It has been found that the grain structures in samples with average grain size greater than 6, i.e., $g>6$ in two dimensions and $g>4$ in three dimensions, provide realistic polycrystalline microstructures [37,38]. We also restrict our analysis to grain sizes for which the ratio g/L is less than $1/10$ to avoid grains which span the sample and to reduce finite-size effects. In two dimensions we present simulations on lattices of up to $L=1000$ and in three dimensions on lattices of up to $L=100$. The most time consuming part of our calculations is the generation of the grain structures. Examples of typical grain structures in two and three dimensions are presented in Figs. 1(a) and 1(b), respectively.

In order to model GBE materials, we consider a fraction c of the grain boundaries to be strong and a fraction $1-c$ to be weak. The bonds across the weak grain boundaries are assigned an energy ϵ, while the bonds which are interior to the grains and the bonds across the strong boundaries are both assigned unit energy. The strong grain-boundary bonds are selected based on the difference in Potts labels at the ends of a bond. That is, in the Potts model, each site has a label $s_i=1\ldots q$. We define the normalized difference between the Potts labels at the sites at each end of a bond to be $d=|s_i-s_j|/q$. If $d<c$, then the bond is a strong bond, while if $d>c$ the bond is a weak bond. We also define the difference in labels modulo q, so that labels 1 and q differ by 1. This definition ensures that all label differences occur with equal probability. An example of a two dimensional system where $c=0.39$ is presented in Fig. 2(a). In this figure, the weak grain boundaries are highlighted as thick grey lines. The remaining grain boundaries are strong. Note that in many ma-

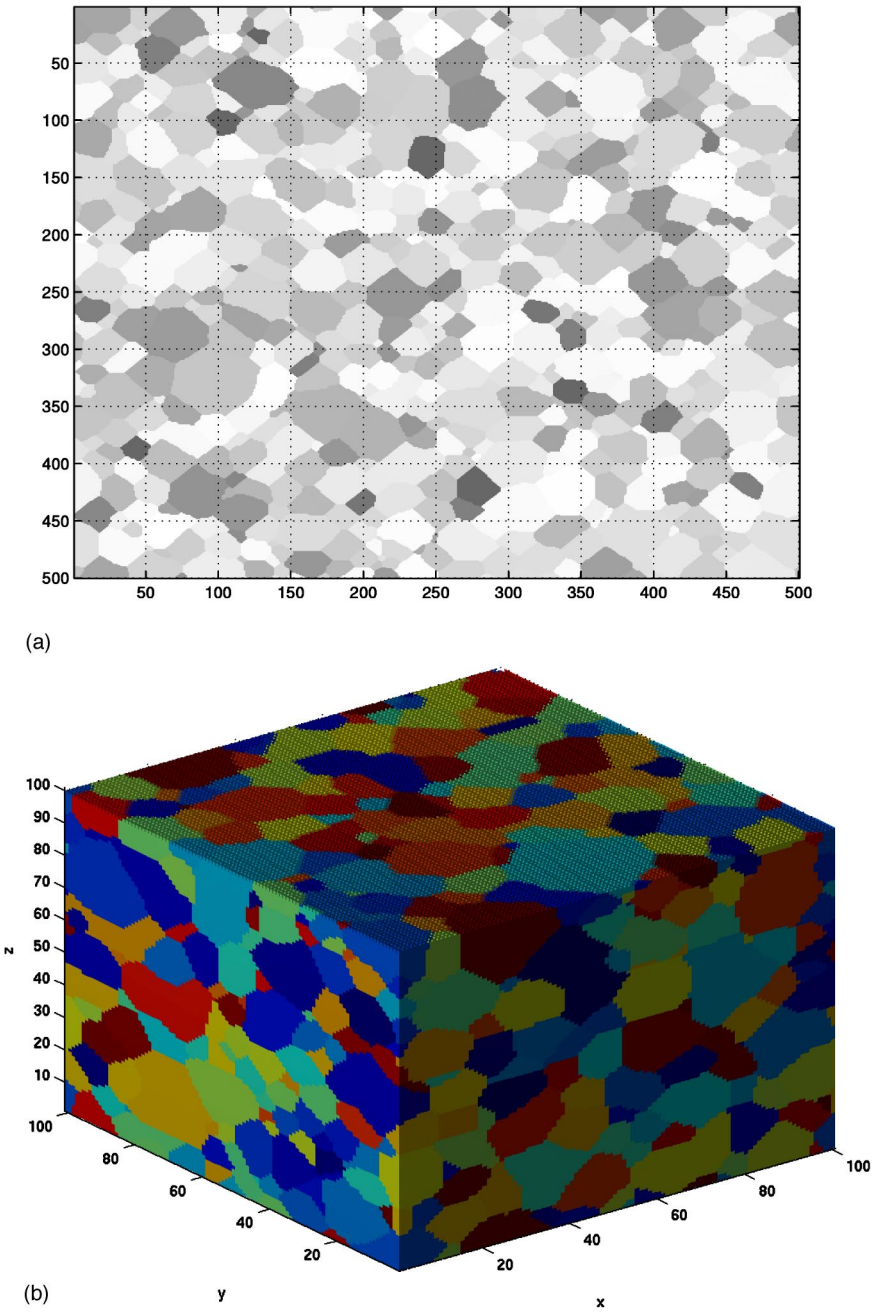

FIG. 1. (Color online) Examples of simulated grain structures in two and three dimensions.

terials the distribution of grain boundary orientations is not uniform, as is implicit in the model used here. The effect of varying the grain-boundary orientation distribution and including correlations in grain-boundary orientations [32] can be included in a straightfoward manner and will be considered elsewhere.

In GBE structural materials there is ample evidence that special boundaries exhibit enhanced corrosion resistance [1–16]. In that application, the ratio of the corrosion resistance of a high angle boundary to that of a special boundary is close to zero. In the case of ceramic superconductors such as YBCO [19] the ratio of critical currents between low and high angle boundaries is of order 100. In GBE materials the ratio of cohesive energies between special and random boundaries is of order 5. For high T_c materials we expect $\epsilon \approx 0.01$, for corrosion $\epsilon \approx 0.0$, while for the cohesive energy of structural materials $\epsilon \approx 0.1$. To span this range of ratios, we present data for the ratios $\epsilon = 0.0001$, 0.01, 0.1 and for the full range of $0 \leqslant c \leqslant 1$. The energy ratio ϵ is a generalized parameter that corresponds to the ratio of critical currents in the high T_c case, the ratio of corrosion resistances in the case of corrosion applications, and to the ratio of cohesive energies in the surface energy application. In the analysis of percolative geometries described below, the specific value of ϵ does not play a role. However, in the calculation of critical manifolds the value of ϵ is important.

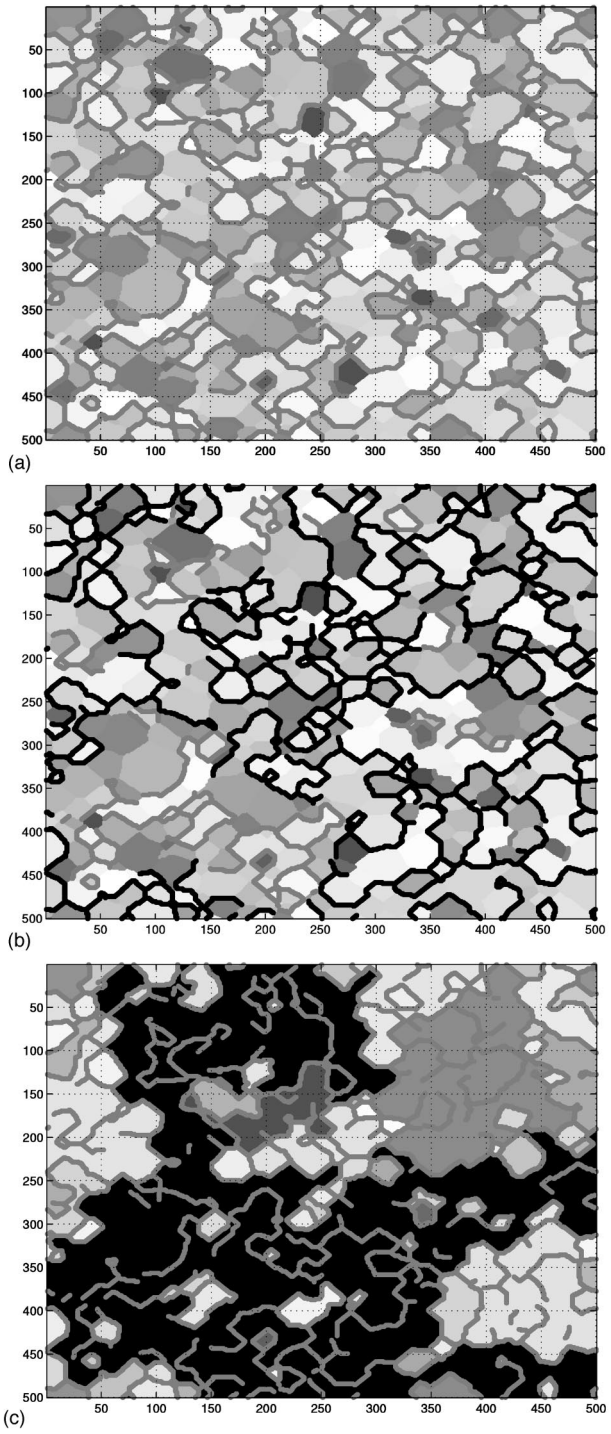

FIG. 2. Illustration of percolation processes in a 2D GBE microstructure. (a) A 2D polycrystalline sample with fraction $1-c=0.61$ of grain boundaries which are weak (thick grey boundary lines). (b) The weak grain boundaries which are connected to the exterior are marked in black. This is the same sample as in (a) and is just above the weak boundary percolation threshold which is on average at $c=0.38(2)$. (c) The strongly connected aggregate is black. This is the same sample as (a). This sample has a percolating strong aggregate and the other colors indicate the different strongly connected clusters.

Two percolation processes are important in the grain-boundary model described above. The first is the onset of a percolating path of weak grain boundaries, which we call weak boundary percolation (WBP). Weak grain boundaries allow the penetration of corrosive agents, e.g., oxygen or steam, into the interior of a material and hence enhance corrosion. It is observed experimentally that three dimensional GBE materials have enhanced corrosion resistance for $c>0.77$ (see, e.g., Fig. 3 of Ref. [12]). In order to find diffusion paths in a polycrystalline microstructure, we use breadth first search starting at the exterior of the sample. This procedure allows penetration from an existing invaded site if the neighboring bond is weak. This invasion is iterated until a surface of strong bonds terminates the penetration process. An example of this penetration process in a two dimensional microstructure with $c=0.39$ is presented in Fig. 2(b). From results such as these we calculate: the probability that a spanning cluster of weak boundaries exists, P_s; and the average penetration depth of weak grain boundaries, l_P. When a spanning cluster of weak boundaries exists, $l_P=L$. In the next section we present data for l_P/L as a function of c.

If a grain is connected to two other grains by strong grain boundaries, then that grain can transmit enhanced mechanical or electrical properties through the network. If there is a continuous path of strongly connected grains, then we have strong aggregate percolation (SAP). We find the largest strong aggregate in polycrystalline microstructures using breadth first search. An example of a strong aggregate in a two dimensional system with $c=0.39$ is presented in Fig. 2(c). In the next section we present data for the spanning probability for this percolation process, P_s, and also the order parameter for this process, which is the probability that a site in the sample is part of the largest strongly connected cluster, γ.

To find the critical manifold through polycrystalline ensembles, we use the push-relabel max-flow/min-cut algorithm of Goldberg and Tarjan [64]. The critical manifold corresponds to the minimum cut in a network flow problem and to the minimal energy surface in a domain wall problem [51]. The minimum cut is associated with the maximum flow in a capacitated network, where in our applications the capacity of each bond is either 1 or ϵ, as described above. This problem is a standard problem in network flow theory and has recently been extensively used to study a variety of statistical physics problems, including the random field Ising model, random manifolds, and periodic elastic media [65]. We have recently used this method to study critical manifolds in polycrystalline materials [50] and we use similar methods to study GBE materials in this work. Examples of minimal energy surfaces found using the maximum flow algorithm for models of GBE materials in two and three dimensions are presented in Figs. 3(a) and 3(b). From results such as these, we calculate the following key properties of the critical manifolds (CM's): The energy of the CM, E; the number of bonds on the CM, N; the fraction of the CM which lies on weak grain boundaries, f_w; and the roughness, $w^2=\langle h^2\rangle-\langle h\rangle^2$ of the CM.

B. Theoretical ideas

Percolation theory is used to describe the scaling behavior near the percolation thresholds c_{WBP} and c_{SAP} [46]. The

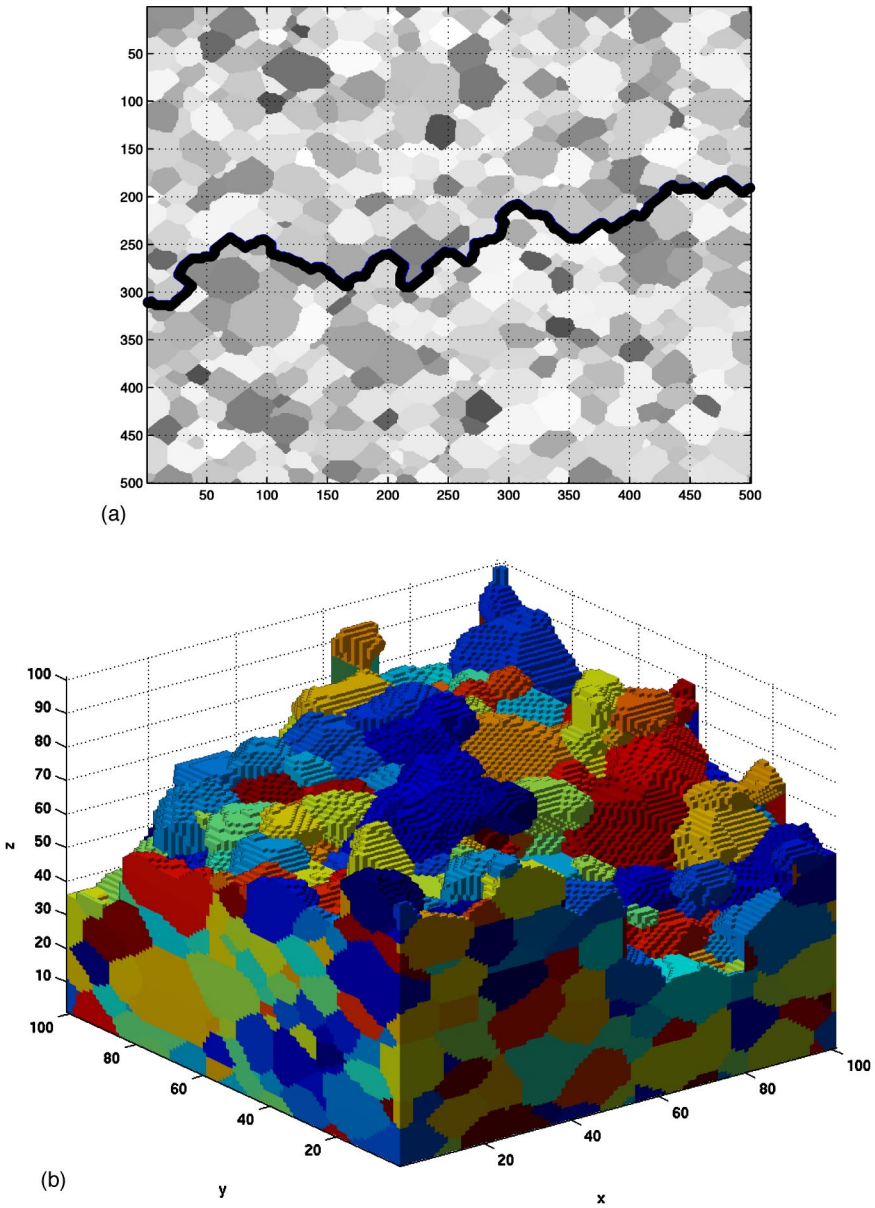

FIG. 3. (Color online) Examples of minimal energy manifolds in two and three dimensions. These examples are for $\epsilon = 0.01$, and (a) a two dimensional system with $c = 0.39$, and (b) a three dimensional sample with $c = 0.15$.

theory of random manifolds is used to describe the scaling behavior of critical manifolds in the regime $c < c_{\mathrm{SAP}}$ [48,57,66], while the theory of periodic elastic media describes the behavior of critical manifolds in the regime $c > c_{\mathrm{SAP}}$ [50,55,57].

First consider the spanning probability P_s, which is the probability that an extensive cluster of connected sites exists in the sample. Above the percolation threshold, $c > c_*$, the spanning probability is 1, $P_s(c > c_*) = 1$, in the thermodynamic limit. Below the percolation threshold, the spanning probability is zero, $P_s(c < c_*) = 0$, in the thermodynamic limit. The width of the transition in P_s, δP_s depends on sample size and goes to zero algebraically as the sample size L goes to infinity,

$$\delta P_s(c_*) \approx (L/g)^{-1/\nu}, \tag{1}$$

where ν is the correlation length exponent, and in two dimensions we have the exact result, $\nu_{2D} = 4/3$, while in three dimensions we have $\nu_{3D} = 0.88$. The effective lattice size of the polycrystalline aggregate is L/g, where g is the average grain size. All of the standard percolation scaling laws [46] are modified by this rescaling. The infinite cluster probability γ is the probability that a site is part of the spanning cluster. In the thermodynamic limit, it behaves as

$$\gamma \approx g^d (c - c_{\mathrm{SAP}})^{\beta} \quad c > c_{\mathrm{SAP}}, \tag{2}$$

where β is the order parameter exponent, which is known exactly in two dimensions, $\beta_{2D} = 5/36$, and to high precision in three dimensions, where $\beta = 0.41$ [46]. The finite size scaling behavior at the critical point is given by

$$\gamma(c_{\mathrm{SAP}}) \approx g^d (L/g)^{-\beta/\nu}. \tag{3}$$

The critical exponents β and ν are expected to be universal, so they apply to both weak boundary percolation and to strong aggregate percolation. The correlation length scales as

$$\xi \approx g|c - c_*|^{-\nu} \tag{4}$$

at both $c_* = c_{\mathrm{WBP}}$ and $c_* = c_{\mathrm{SAP}}$. Of course the prefactors for these two cases are nonuniversal and need to be determined from simulations or experiment.

The penetration depth, which we take to be the largest depth to which weak grain boundaries penetrate, scales as

$$l_P \approx \xi \quad c > c_{\mathrm{WBP}}. \tag{5}$$

Due to the fact that we take the largest penetration depth in our definition of l_P, this quantity has also a logarithmic size dependent correction factor arising from rare fluctuations [67]. An alternative definition of the penetration depth is to take the average depth to which weak boundaries penetrate. This also diverges at the critical threshold, however, with a different exponent and it does not exhibit rare fluctuation effects.

Random manifolds arise in the study of domain walls in random bond Ising magnets. The scaling behavior of these domain walls has been elucidated in Refs. [48] and [66]. Two key properties in this analysis are the energy of the domain walls and the roughness of the domain walls. The scaling laws obeyed by continuum models for random bond Ising models are

$$E = a_1 L^{d-1} + a_2 L^{\theta} \quad \text{and} \quad w = a_3 L^{\zeta}, \tag{6}$$

where a_1, a_2, a_3 are nonuniversal constants, d is the spatial dimension, L is the sample size, and θ and ζ are universal exponents which are related by the equation $\theta = 2\zeta + d - 3$ [48,56,65,66]. The value of ζ is known to be exactly $2/3$ in two dimensions [48] and to be approximately $\zeta = 0.41(1)$ [51,66] in three dimensions. The scaling behavior of critical manifolds in GBE materials are described by similar scaling laws in the limit $c < c_{\mathrm{SAP}}$ as will be demonstrated in Sec. IV.

In the $\langle 100 \rangle$ orientation domain walls of random bond Ising magnets on cubic lattices, the lattice structure imposes a periodic potential on the random manifold. Random manifolds in a periodic potential arise in a variety of other contexts and the term "periodic elastic media" has been coined to describe models of these phenomena. The scaling laws for periodic elastic media (PEM) are quite simple generalizations of the scaling laws presented in Eq. (6). Random manifolds in PEM exhibit a competition between the tendency of the periodic potential to pin the manifold and to make it flat, and the tendency of the disorder to make the manifold rough. Scaling theories of periodic elastic media [55–57] indicate that in hypercubic lattices in the $\langle 10 \rangle$ or $\langle 100 \rangle$ directions, the critical length L_c beyond which manifolds roughen scales as

$$L_c \approx p/(1-p) \quad \text{and} \quad L_c \approx \exp[a_0 p/(1-p)] \tag{7}$$

in two and three dimensions, respectively [57]. In these equations p is the probability that a bond is present in a hypercubic lattice and a_0 is a constant. The scaling laws for the energy and roughness of PEM's are then modified to

$$E = a_5 L^{d-1} + a_6 L^{\theta} \quad \text{and} \quad w = a_7 \left(\frac{L}{L_c} \right)^{\zeta}. \tag{8}$$

The new feature in comparison with Eq. (6) is the appearance of L_c in the scaling of the roughness. Physically, L_c is the typical size of flat regions on the critical manifold or domain wall. The critical length L_c is important in modeling critical manifolds in GBE materials in the regime $c > c_{\mathrm{SAP}}$, and in Sec. IV, we extend the analysis of L_c to the case of GBE materials and show that the scaling behavior of all of the properties we calculate numerically can be related to the scaling behavior of this critical length.

III. PERCOLATION PROCESSES

Figures 4 present data for the spanning probability for weak boundary percolation (solid symbols) and strong aggregate percolation (open symbols) in two dimensions [see Fig. 4(a)] and in three dimensions [see Fig. 4(b)]. First consider the two dimensional data in Fig. 4(a). A simple model for this case is to assume that the polycrystalline microstructure consists of a regular infinite lattice of hexagons each of size proportional to the average grain size g. The percolation thresholds in that case are known exactly. The weak boundary percolation process is equivalent to bond percolation on a honeycomb lattice, while the strong aggregate percolation corresponds to bond percolation on the dual to the honeycomb lattice, which is the triangular lattice. From this we deduce that the strong aggregate and weak bond percolation thresholds are equivalent in regular honeycomb lattices and that $c_{\mathrm{SAP}} = c_{\mathrm{WBP}} = 2\sin(\pi/18) \approx 0.347\ldots$ [46]. The data in Fig. 4(a) are quite consistent with this result, though the percolation threshold is shifted slightly to higher values of c. Taking the crossing point of the curves in Fig. 4(a) as an indicator of the percolation threshold, we find $c^{2D}_{\mathrm{SAP}} = 0.38(1)$ and $c^{2D}_{\mathrm{WBP}} = 0.38(1)$. One possible origin for the slightly higher threshold in the polycrystalline model as compared to the regular honeycomb lattice is the presence of some fourfold grain-boundary junctions in the polycrystalline network.

Figure 4(b) presents the data found for P_s in three dimensions. The most obvious difference between the results in Fig. 4(a) and those in Fig. 4(b) is that in three dimensions, the onset of a strong aggregate occurs well before the cessation of percolation of weak grain boundaries. This means that there is a broad regime in which an "interpenetrating phase" exists. In this phase an extensive strong aggregate co-exists with percolation of weak boundaries. In two dimensional grain structures this cannot occur as the percolation of weak boundaries cuts off the percolation of a strong aggregate. From the results in Fig. 4(b), we find that $c^{3D}_{\mathrm{SAP}} = 0.12 \pm 0.03$ and $c^{3D}_{\mathrm{WBP}} = 0.77 \pm 0.03$. A grain in a three dimensional (3D) polycrystalline network typically has 12–14 neighboring grains. The rhomboid dodecahedral lattice (i.e., fcc) is quite similar in topology. The fcc strong aggregate and weak bond percolation thresholds are $c_{\mathrm{WBP}} = 0.802$ and $c_{\mathrm{SAP}} = 0.119$ [46], which are actually quite close to the values which we observe in the simulations.

Figure 5 presents data for order parameters related to the two key percolation processes in our GBE models. The first order parameter is related to percolation of the strong aggregate. The order parameter in this case is the probability that a site is on the largest strongly connected cluster γ (solid symbols in Fig. 5). The order parameter for the onset of a

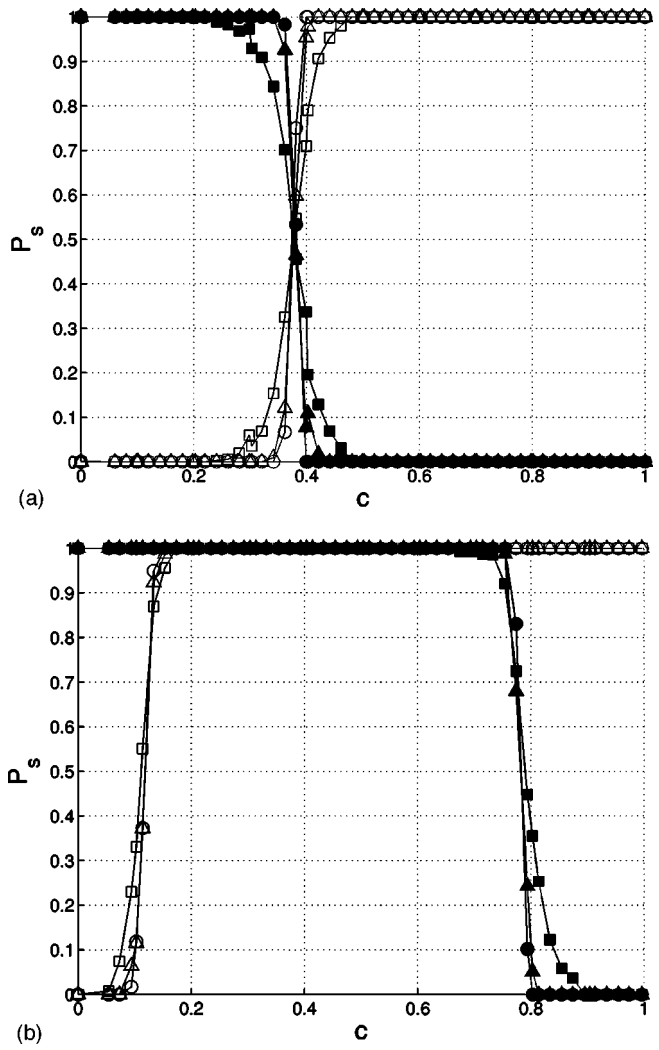

FIG. 4. The spanning probabilities P_s for weak boundary percolation (solid symbols) and strong aggregate percolation (open symbols) as a function of the concentration of strong grain boundaries c in (a) two dimensions and (b) three dimensions. In each case, the data are averaged over a range of values of the effective lattice size L/g. The open and filled squares are from averages over the range $10 \leqslant L/g \leqslant 50$ (two dimensions) and $6 \leqslant L/g \leqslant 10$ (three dimensions); the open and filled triangles are from averages over $50 \leqslant L/g \leqslant 100$ (two dimensions) and $10 < L/g < 15$ (three dimensions); the open and filled circles are from averages over $100 \leqslant L/g \leqslant 200$ (two dimensions) and $15 < L/g < 20$ (three dimensions). The two dimensional data were calculated from a total of over 30 000 different polycrystalline samples, while the three dimensional data were calculated using over 15 000 samples.

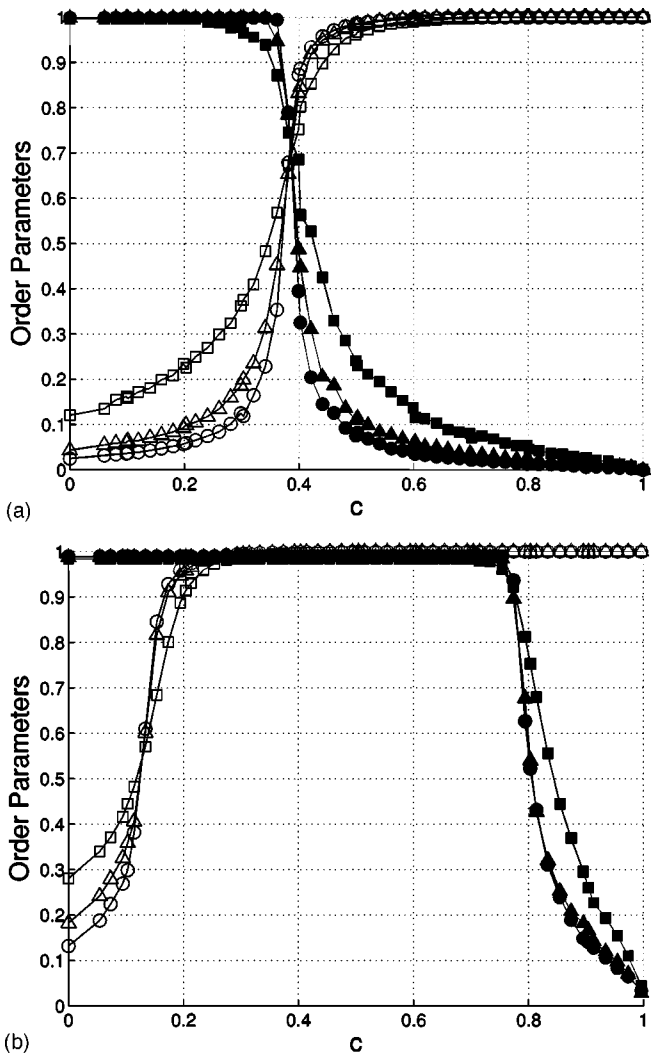

FIG. 5. Two order parameters for the two different percolation processes occuring in the GBE model. The order parameter for strong aggregate percolation is the infinite cluster probability (open symbols) which has the scaling behavior given by Eq. (2). The order parameter for weak boundary percolation is the penetration depth of the weak boundaries (solid symbols). The scaling behavior of this order parameter is given by Eqs. (4) and (5). Results are presented for three different sample sizes and in (a) two dimensions and (b) three dimensions. The data are averaged in the same way as that described in the caption to Fig. 4

percolating weak boundary network is the penetration depth of weak grain boundaries l_P (open symbols in Fig. 5). As expected, the thresholds for these order parameters are consistent with the results found from the spanning probability. The scaling exponents for γ and l_P are expected to be those given in Eqs. (2) and (5), respectively, and we find that the standard exponents are consistent with the data of Fig. 5. As a practical matter, the penetration of corrosive agents into a material is suppressed strongly for $c > c_{\mathrm{WBP}}$ due to the rapid decrease in l_P for $c > c_{\mathrm{WBP}}$ (see Figs. 5).

IV. CRITICAL MANIFOLDS

We have calculated four properties of CM's as a function of c, the concentration of strong bonds, and the bond contrast ϵ. Note that we take both the energy of the strong boundaries and that of the grain interiors to be unity, so that ϵ is the ratio between the strength of the weak boundary bonds and either of these bonds. The properties we have calculated are: (i) the energy of the CM, E; (ii) the fraction of the CM which lies on weak grain boundaries, f_w; (iii) the total number of bonds which lie on the CM, N; and (iv) the roughness of the CM, w. The results that we have found for these four quantities in two and three dimensions are presented in Figs. 6–9. In order to understand the results presented in Figs. 6–9, we develop

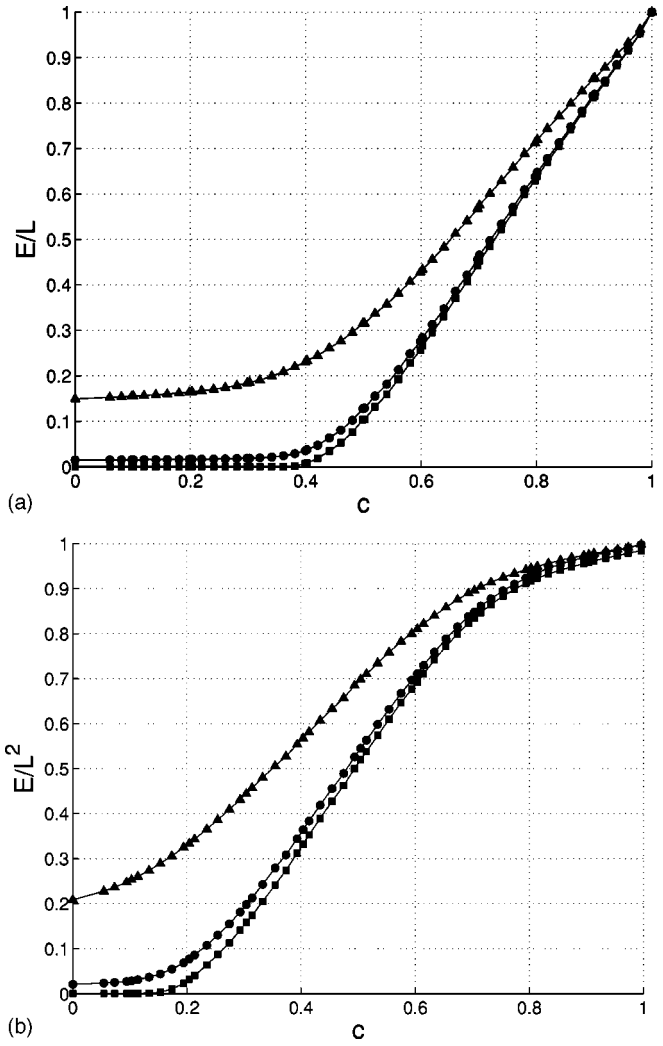

FIG. 6. The average interface energy as a function of strong bond concentration for three values of the bond strength ratio, $\epsilon = 0.0001$ (filled squares), $\epsilon = 0.01$ (filled circles), $\epsilon = 0.1$ (filled triangles) in (a) two dimensions and (b) three dimensions. The data are averaged over a range of values of L/g, which is the effective lattice size. In two dimensions we restricted calculations to effective lattice sizes in the range $100 < L/g < 200$, while in three dimensions we considered $15 < L/g < 20$. These effective lattice sizes are quite small, so we expect finite size effects to be significant. In two dimensions the data come from averaging over a total of 3480 samples, while in three dimensions the total number of samples in the selected window was 3422.

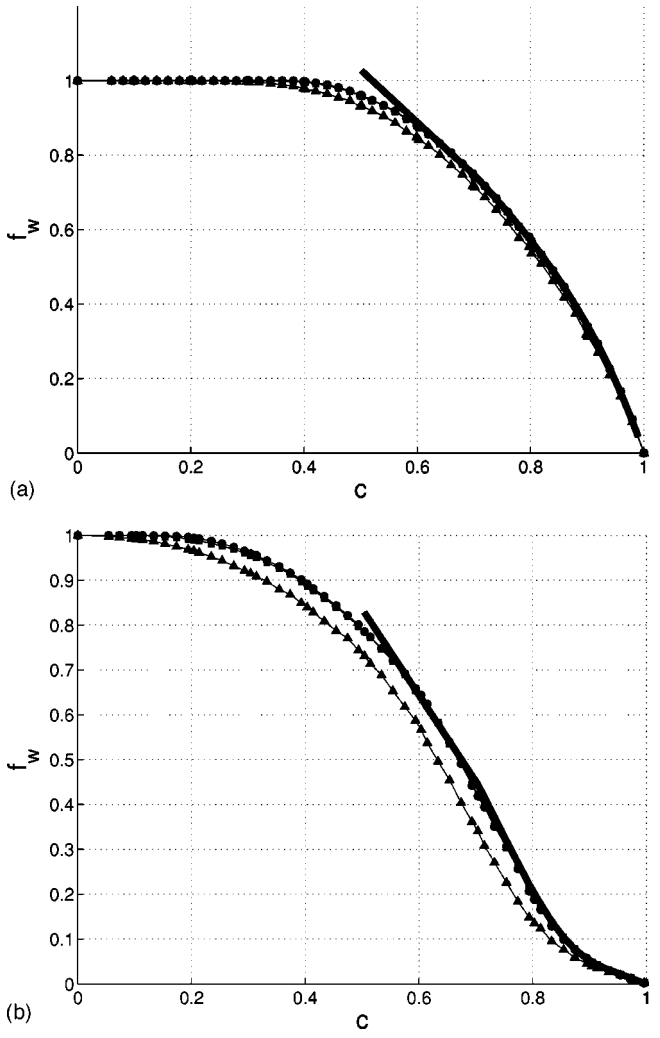

FIG. 7. The fraction of the critical manifold which consists of weak grain boundaries as a function of strong bond concentration for CM's in: (a) two dimensions and (b) three dimensions for $\epsilon = 0.0001$ (filled squares), $\epsilon = 0.01$ (filled circles), and $\epsilon = 0.1$ (filled triangles). The data are averaged the same as was described in the caption to Fig. 6. The heavy lines are fits of the $\epsilon = 0.0001$ data to the scaling predictions of Eqs. (33) and (34) in the concentration range $0.7 < c < 1.0$. In (a), the parameter values $a_1 = 1.58$, $a_2 = 0.56$, and $a_3 = 0.19$ were used in Eq. (33) to obtain the fit, while in (b), the parameter values $a_1 = 0.46$, $a_2 = 3.22$, $a_3 = 0.50$, and $b_0 = 0.53$ were used in Eq. (34). The curve of best fit is presented in the interval $c > 0.5$ for illustration purposes.

scaling laws in three regimes: $c \approx c_{\mathrm{SAP}}$, $c \ll c_{\mathrm{SAP}}$, and $c \gg c_{\mathrm{SAP}}$. We concentrate on the regime $\epsilon \leqslant 0.1$ which is of most interest for GBE applications.

A. Low concentrations $c \ll c_{\mathrm{SAP}}$

At low concentrations of strong grain boundaries, and provided the energy ratio ϵ is small, the CM lies almost entirely on the weak grain boundaries, as found in models of polycrystalline materials [50]. This is evident in Fig. 7 which gives the fraction of the CM bonds which lie on weak grain boundaries. For $c \ll c_{\mathrm{SAP}}$, $f_w \approx 1$ and this leads to simple behaviors for all of the quantities that we measure. First, the energy of the CM is simply

$$E \approx \epsilon L^{d-1} \approx \epsilon N. \tag{9}$$

That is, since all of the CM bonds lie on weak grain boundaries, the CM energy is the number of bonds on the CM times the energy contrast. A plot of the scaled energy E/L^{d-1} as a function of c is presented in Fig. 6. It is evident that the scaling behavior of Eq. (9) extends all the way to c_{SAP} as is expected based on the fact that f_w remains near unity for $c < c_{\mathrm{SAP}}$.

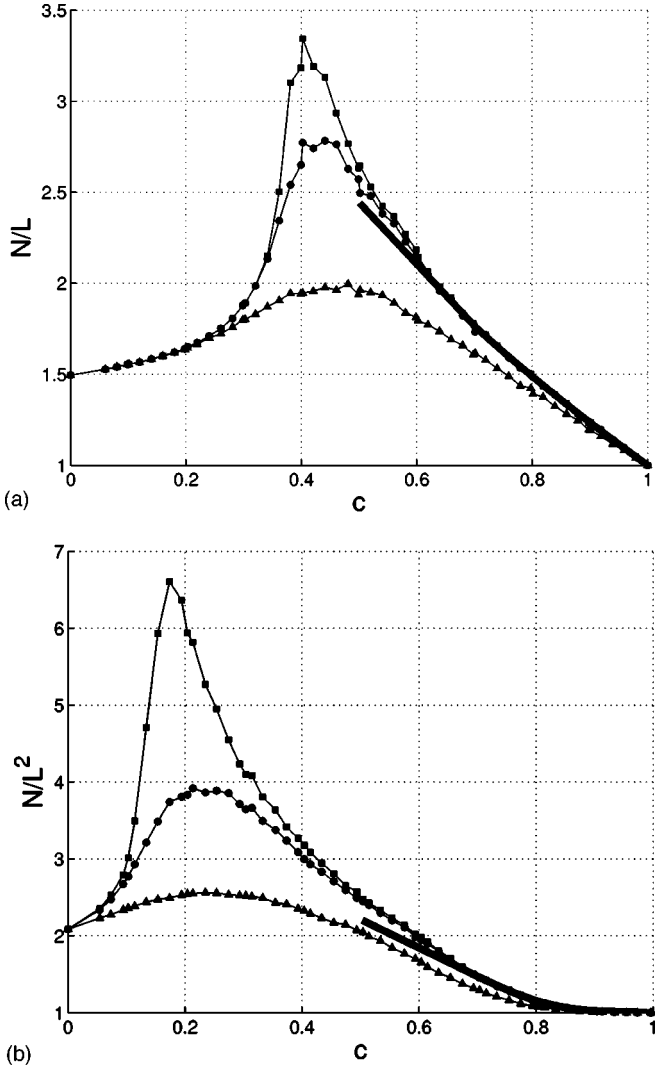

FIG. 8. The total number of bonds which lie on the critical manifold N as a function of the strong bond concentration c for three values of the bond strength ratio, $\epsilon=0.0001$ (filled squares), $\epsilon=0.01$ (filled circles), and $\epsilon=0.1$ (filled triangles). (a) The data in two dimensions; (b) the data in three dimensions. The data are averaged the same as was described in the caption to Fig. 6. The heavy line is a fit of the $\epsilon=0.0001$ data to the scaling theory predictions of Eqs. (36) and (37) in the interval $0.7<c<1.0$. In (a), the parameter values $a_1=1.69$ and $a_2=0.59$ were used in Eq. (36) to obtain the fit, while in (b), the parameter values $a_1=0.22$, $a_2=4.36$, and $b_0=0.68$ were used in Eq. (37). The curve of best fit is presented in the interval $c>0.5$ for illustration purposes.

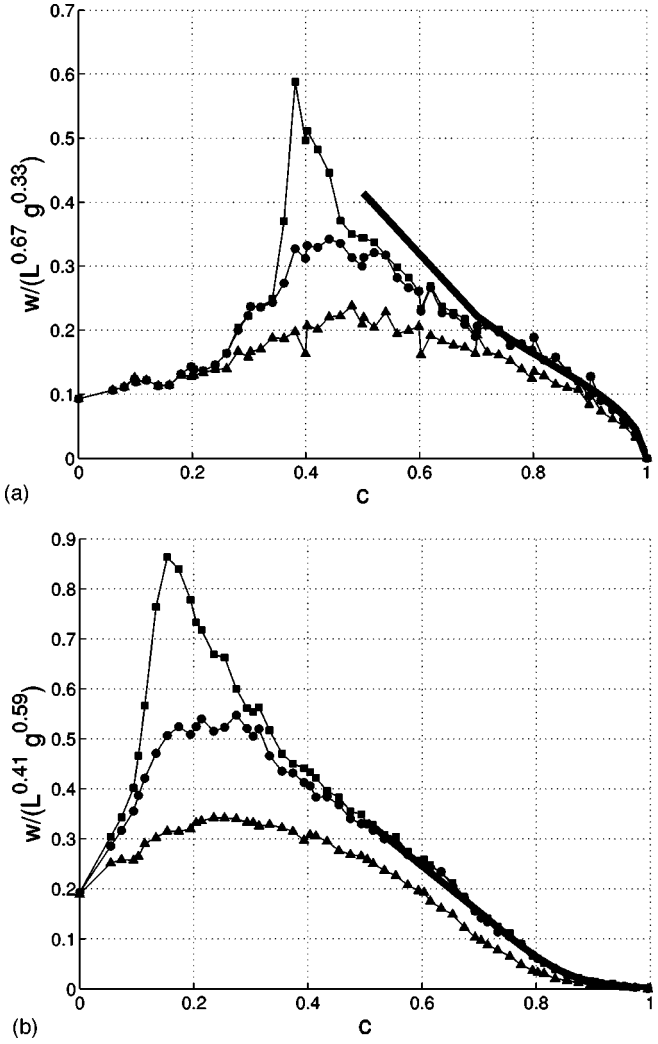

FIG. 9. The scaled roughness as a function of the strong bond concentration for three values of the bond strength ratio, $\epsilon=0.0001$ (filled squares), $\epsilon=0.01$ (filled circles), and $\epsilon=0.1$ (filled triangles). The data are averaged in the same way as described in the caption to Fig. 6. The heavy line is a fit of the $\epsilon=0.0001$ data to the scaling theory predictions of Eqs. (30) and (31) in the interval $0.7<c<1.0$. In (a), the parameter values $a_1=0$, $a_2=0.36$, and $\zeta=0.59$ were used in Eq. (30) to obtain the fit, while in (b), the parameter values $a_1=0.12$, $a_2=0.67$, $b_0=1.48$, and $\zeta=0.41$ were used in Eq. (31). The curve of best fit is presented in the interval $c>0.5$ for illustration purposes.

The roughness of the CM in the low concentration limit is the same as that of random manifolds in polycrystalline materials in the limit of weak boundaries, $\epsilon \ll 1$, so that [50]

$$w \approx g\left(\frac{L}{g}\right)^{\zeta}, \tag{10}$$

where ζ is the roughness exponent [see Eq. (6) and the discussion following it]. The roughness of the CM as a function of grain size, at fixed sample size L, is then predicted to be $w \propto g^{1-\zeta}$. Tests of this relation in two and three dimensions are presented in Fig. 10. The exponents found are nicely consistent with the expected universal values $\zeta_{2D}=2/3$ and $\zeta_{3D}=0.41(1)$ [51,52]. This lends strong support to the idea that L/g acts as an effective lattice constant for CM's in polycrystalline materials.

B. Critical regime $c \approx c_{\mathrm{SAP}}$

Percolative effects dominate in the critical regime, and the scaling behavior may be understood based on critical scaling and finite size scaling near second-order phase transitions.

First consider the case $\epsilon \to 0$, in which case the finite-size scaling behaviors at c_{SAP} are given by

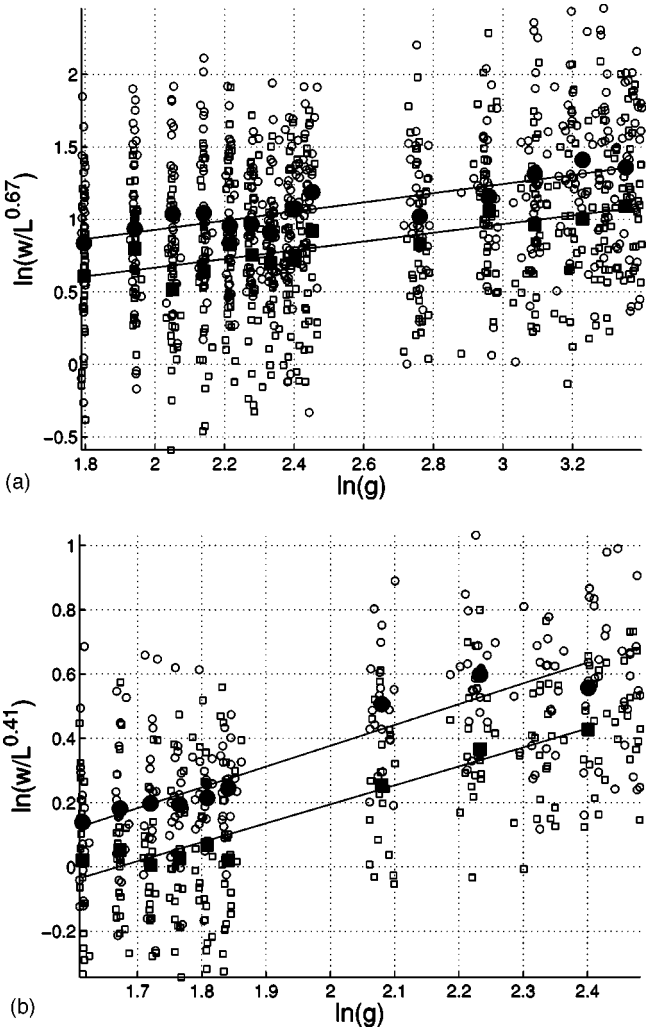

FIG. 10. Scaling of the roughness as a function of grain size: (a) in two dimensions for $c=0.3$ and $c=0.5$; (b) in three dimensions for $c=0.1$ and $c=0.35$. The open circles are the raw data at $c=0.3$ (two dimensions) and $c=0.1$ (three dimensions). The open squares are the raw data at $c=0.5$ (two dimensions) and at $c=0.35$ (three dimensions). The filled circles and filled squares are the data averaged over a narrow bin (of order 1) in grain size. The lines of best fit to the data are indicated. In both two and three dimensions the data agree well with the scaling prediction of Eq. (18). In two dimensions the line of best fit has a slope 0.30(2) for $c=0.3$ and 0.32(2) for $c=0.5$ while in three dimensions we find a slope of 0.59(5) for $c=0.1$ and a slope of 0.65(5) at $c=0.35$, which should be compared with the prediction $g^{1-\zeta}$, where $1-\zeta=1/3$ in two dimensions and $1-\zeta=0.59$ in three dimensions.

$$E \approx 1; \quad w \approx L; \quad N \approx L^{D_e}, \tag{11}$$

where D_e is the external perimeter dimension in percolation. In two dimensions, $D_e=5/4$ [46], while in three dimensions $D_e=D_f$ where $D_f=2.53$ is the fractal dimension of the infinite cluster [46]. At the critical point, the number of bonds on the CM is proportional to the number of bonds on the external perimeter of the largest strong-aggregate cluster, as the CM avoids cutting any strong bonds in the small ϵ limit. The energy result in Eq. (11) is evident from the fact that on the infinite cluster there are singly connected bonds which may be cut to disconnect the cluster. The roughness is of order of the sample size due to the fact that the infinite cluster is an isotropic fractal with holes on all length scales. The behavior on approach to p_c is found by using the nodes, links, and blobs picture [46] to rewrite Eq. (11) as

$$\frac{E}{L^{d-1}} \approx \frac{1}{\xi^{d-1}}; \quad \frac{N}{L^{d-1}} \approx \xi^{D_e-d+1}; \quad w \approx \xi\left(\frac{L}{\xi}\right)^{\zeta}, \tag{12}$$

where $\xi \approx g|c-c_{\mathrm{SAP}}|^{-\nu}$ is the correlation length. From these equations, we find

$$\frac{E}{L^{d-1}} \approx (c-c_{\mathrm{SAP}})^{(d-1)\nu}, \quad c > c_{\mathrm{SAP}}, \tag{13}$$

$$w \approx g^{1-\zeta}L^{\zeta}|c-c_{\mathrm{SAP}}|^{-\nu(1-\zeta)} \quad L \gg \xi, \tag{14}$$

and

$$\frac{N}{L^{d-1}} \approx (c-c_{\mathrm{SAP}})^{-(D_e-d+1)/\nu} \quad L \gg \xi. \tag{15}$$

However, if the energy contrast ϵ is finite, the divergence in the roughness at c_{SAP} is rounded. This is due to the fact that in that case, large excursions of the critical manifold cost an energy proportional to the number of bonds in the excursion times ϵ. If the energy of a large excursion around strongly connected grains is larger than the cost of breaking the grain, then cleavage of the grain occurs. If we define r to be the length scale of the excursion, then the energy cost of an excursion is proportional to $\epsilon g^{d-1}r^{D_e}$.

Equating this to the energy cost of cleaving a grain g^{d-1}, we find a critical length for cleavage r_c, given by

$$r_c \approx \frac{1}{\epsilon^{1/D_e}}. \tag{16}$$

If the percolative correlation length is much greater than the length scale cutoff given by Eq. (16), i.e., $\xi \gg r_c$, then the energy of the CM is given by

$$E \approx g^{d-1}\left(\frac{L}{gr_c}\right)^{d-1} \propto (\epsilon)^{(d-1)/D_e}L^{d-1}. \tag{17}$$

As seen in Figs. 8 and 9, at finite energy contrasts, the number of bonds on the CM and the roughness of the CM are reduced dramatically. This is understood as follows. The largest possible excursion of the CM at finite ϵ is gr_c. The roughness of the CM then scales as gr_c instead of with ξ. In a similar way, the number of bonds on the interface also scales with gr_c. In particular for the roughness, we expect that the roughness is that of a random manifold with renormalized lattice size L/gr_c, so that

$$w \approx gr_c\left(\frac{L}{gr_c}\right)^{\zeta} = \epsilon^{(\zeta-1)/D_e}g^{1-\zeta}L^{\zeta}. \tag{18}$$

The roughness thus diverges as the energy contrast goes to zero as $w \approx \epsilon^{-0.267}$ in two dimensions where $\zeta=2/3$, $D_e=5/4$, while $w \approx \epsilon^{-0.233}$ in three dimensions where $\zeta=0.41(1)$, $D_e \approx 2.53$. The exponents describing the scaling of roughness with the energy ratio ϵ are quite small, which

indicates that a large energy contrast is required in order to observe pronounced peaks in the roughness and in the number of bonds on the CM near c_{SAP}. This is evident from Figs. 7 and 8, where it is seen that even for a contrast of $\epsilon=0.01$, the critical behavior near c_{SAP} is rounded significantly. The energy and the fraction of weak boundaries on the CM are more weakly dependent on the energy contrast (see Figs. 5 and 6), though as seen in Eq. (17) there are still nontrivial scaling laws at c_{SAP}.

Another feature of the behavior of w and N as a function of strong bond concentration is that the peak value of these quantities moves to higher c as the energy contrast ϵ increases. This is due to the fact that at finite ϵ, the maximum manifold wandering occurs when $c>c_{\mathrm{SAP}}$ and $r_c=\xi$. These conditions maximize the number of strong bonds while still providing weak paths up to length r_c. Using these conditions, we find that the peak in the roughness and in the number of CM bonds occur at c_P found from

$$\frac{1}{\epsilon^{1/D_e}} = (c_P - c_{\mathrm{SAP}})^{-\nu}. \tag{19}$$

The location of the peak shift thus scales as

$$c_P - c_{\mathrm{SAP}} \approx \epsilon^{\nu/D_e}. \tag{20}$$

C. High concentrations, $c \gg c_{\mathrm{SAP}}$, $\epsilon \to 0$

The limit $c=1$ is trivial, as in that limit the CM is a cleavage surface, so that the number of bonds on the CM is just the surface area and the energy is N times the energy of the strong bonds, which we have taken to be 1. The roughness of a flat surface is zero and the fraction of the CM that is on weak boundaries is clearly zero. For $c=1$, we thus have

$$\frac{E}{L^{d-1}} = \frac{N}{L^{d-1}} = 1; \quad \text{and} \quad f_w = 0 = w. \tag{21}$$

In the regime $c<1$ with $1-c$ small, we can consider there to be a relatively small number of weak grain boundaries. This is the regime in which scaling concepts used in the analysis of periodic elastic media apply. We are primarily interested in the limit of small values of ϵ, so that a weak boundary is favorable at almost all angles to the average CM plane. For finite $1-c$ an Imry-Ma argument provides a surprisingly good theory to describe the large scale behavior of the critical manifold.

In the analysis below, we use the renormalized length scale $l=L/g$. In the Imry-Ma argument [55,57], we consider a fluctuation of size l from a flat surface. This fluctuation consists of l^{d-1} grain boundaries. Such a fluctuation is advantageous if it contains a larger than average number of weak grain boundaries. The large scale roughening of the critical manifold is driven by the nonperturbative or "co-operative" Imry-Ma fluctuations which in the context of GBE materials are derived and analyzed below. In addition to these large scale excitations, there are small scale fluctuations which lead to terms proportional to $1-c$. These terms can be considered to be perturbative terms while the Imry-Ma terms are nonperturbative.

According to the central limit theorem, the probability that a fluctuation of size S has energy E_S is given by

$$P(E_S) \propto \frac{1}{(2\pi\sigma^2 S)^{1/2}} e^{-(E_S - e_\infty S)^2/[2\sigma^2 S]}, \tag{22}$$

where $S=l^{d-1}$ is the number of grains in the fluctuation. Here E_S is in units of the grain size. To recover the energy of the fluctuation in standard units, we just multiply E_S by g^{d-1}. e_∞ is the average energy (per grain) of a grain boundary while σ^2 is the standard deviation (per grain) in the energy of a grain boundary. For the GBE model we are using, we have

$$e_\infty = c; \quad \sigma^2 = c(1-c). \tag{23}$$

From Eq. (22) we estimate the typical size of the largest energetically favorable fluctuation by finding the solution to

$$\frac{1}{(2\pi\sigma^2 S)^{1/2}} e^{-\delta E_{\mathrm{gain}}^2/(2\sigma^2 S)} \approx 1. \tag{24}$$

The maximum energy gain achieved by these fluctuations is then proportional to

$$\delta E_{\mathrm{gain}} \propto [\sigma^2 S \ln(2\pi\sigma^2 S)]^{1/2}. \tag{25}$$

The energy cost of such a fluctuation scales as

$$\delta E_{\mathrm{cost}} \propto e_\infty l^{d-2}. \tag{26}$$

From Eqs. (25) and (26) it is evident that at large enough length scales, the energy gain is larger than the energy cost in both two and three dimensions. The energy gain favors a fluctuation which roughens the critical manifold, so at long length scales, the critical manifold "wanders" to take advantage of regions of the material where there is a larger than average number of weak boundaries. The most important quantity in the theory is the critical length L_c, which is the length scale at which the wandering sets in. The critical manifold is flat on length scales $L<L_c$ and "rough" on longer length scales, i.e., it is rough for $L>L_c$. Equating Eqs. (25) and (26) and dropping the logarithmic term leads to the following result for critical manifolds in two dimensional systems, such as thin films:

$$\sigma^2 S \approx e_\infty^2, \quad \text{so that} \quad L_c \approx \frac{gc}{(1-c)}. \tag{27}$$

In three dimensions, i.e., for bulk materials, the logarithmic term in Eq. (25) is dominant and must be kept, which results in the expression

$$\sigma^2 \ln(2\pi\sigma^2 S) \approx e_\infty^2, \quad \text{so} \quad L_c \approx g \frac{\exp\left[b_0 \frac{c}{1-c}\right]}{[c(1-c)]^{1/2}}, \tag{28}$$

where b_0 is a nonuniversal constant. The critical length L_c diverges much more rapidly as $c \to 1$ in three dimensions than in two dimensions. This means that critical manifolds are more prone to cleavage in three dimensions than in two dimensions, for the same degree of grain-boundary engineering. The theory leading to the algebraic prefactor of the three dimensional result may have two other logarithmic corrections. The first is due to the number of ways in which a CM fluctuation may be placed in the material. This leads to an

additional factor of l multiplying the left-hand side of Eq. (24). In addition, the energy cost equation (26) may be reduced by a factor of $\ln L$. These logarithmic factors do not affect the result in two dimensions or the exponential term in the three dimensional result. However, they do affect the algebraic prefactor in the three dimensional result. The way in which they modify the three dimensional result is incorporated into the more general form $L_c = g[c(1-c)]^{-y} \exp[b_0 c/(1-c)]$, where the new exponent y depends on the details of the model, but is less than or equal to 1. In comparing with numerical data, we considered several values of y, but found that $y=1/2$ provides an adequate description of the data. This is the case stated in Eq. (28) and in the results which follow from it.

From the critical length L_c we deduce the behavior of the four CM properties which we measure. First, the co-operative or nonperturbative contribution to the roughness of CM's is given by

$$w \approx g\left(\frac{L}{L_c}\right)^{\zeta} \quad \text{so that} \quad \frac{w}{L^{\zeta} g^{1-\zeta}} \propto \frac{1}{l_c^{\zeta}}, \tag{29}$$

where $l_c = L_c/g$. At fixed g and L, we then find that in two dimensions [using Eq. (27)], for $c \gg c_{\mathrm{SAP}}$, w behaves as

$$\frac{w}{g^{1-\zeta} L^{\zeta}} \approx a_1(1-c) + a_2\left(\frac{1-c}{c}\right)^{\zeta}. \tag{30}$$

The first term in this expression is the perturbative term due to the small deviations of the CM from the flat manifold. The second term is the co-operative term, and is due to large Imry-Ma deviations from the flat CM. In three dimensions a similar discussion yields

$$\frac{w}{g^{1-\zeta} L^{\zeta}} \approx a_1(1-c) + a_2[c(1-c)]^{\zeta/2} e^{-b_0 \zeta c/(1-c)}. \tag{31}$$

In both two and three dimensions a_2 is expected to be independent of g and L except for finite size scaling corrections. However, a_1 is expected to be size dependent due to the normalization of w. The perturbative correction should scale as $w \approx a_1' g(1-c)$, with a_1' a size independent constant. At large sample sizes, we thus expect a_1 to go to zero. However, for finite grain sizes and relatively small sample sizes, there is a significant linear term. The co-operative contribution to the roughness of CM's approaches zero algebraically in two dimensions and exponentially in three dimensions. This is typical of the behavior of periodic elastic media in the weak disorder limit, where roughening of manifolds only occurs at exponentially large length scales [55]. The forms (30) and (31) are compared to the data of Figs. 9(a) and 9(b) from which it is evident that they provide a good representation of the behavior in the large c limit.

Now we consider the fraction of the weak grain boundaries which lie on the CM. The average number of weak boundaries on a cleavage plane is $f_w \approx a_1(1-c)$. In addition, when the critical manifold wanders, it wanders to regions of the material where there is an excess of weak boundaries δf_w. This is the origin of the co-operative term discussed above. The typical value of the co-operative term δf_w is described by the same statistics as the energy fluctuations, so that

$$\delta f_w \approx \sigma l_c^{(d-1)/2} / (l_c^{d-2} + l_c^{d-1}), \tag{32}$$

where $l_c = L_c/g$. The term in the denominator is the total number of grain boundaries in the favorable fluctuation. Using Eq. (27) the behavior of f_w in the large c limit for two dimensional systems (thin films) is predicted to be

$$f_w \approx a_1(1-c) + a_2' \frac{\sigma l_c^{1/2}}{1+l_c} \approx a_1(1-c) + \frac{a_2 c}{1 + a_3 \frac{c}{1-c}}, \tag{33}$$

where a_1, a_2, a_3 are nonuniversal constants. The first term in Eq. (33) is the perturbative term, while the second term is the co-operative term. In three dimensions a similar argument yields

$$f_w \approx a_1(1-c) + \frac{a_2[c(1-c)]^{1/2}}{1 + a_3 \frac{e^{b_0 c/1-c}}{[c(1-c)]^{1/2}}}, \tag{34}$$

where a_1, a_2, a_3, b_0 are nonuniversal constants and the co-operative term is proportional to $\sigma/(1+l_c)$, from Eq. (32). These forms are compared to the numerical data in Figs. 7 from which it is seen that they provide a good representation of the data.

The co-operative contribution to the number of bonds on the CM is approximately

$$N \approx (g L_c^{d-2} + L_c^{d-1}) \left(\frac{L}{L_c}\right)^{d-1}. \tag{35}$$

This leads to $N/L^{d-1} = 1 + 1/l_c$. Adding the linear term to this co-operative term, the result for two dimensions is found to be

$$\frac{N}{L} \approx 1 + a_1(1-c) + a_2(1-c)/c, \tag{36}$$

where a_1, a_2 are nonuniversal constants. Again the first term is the perturbative term, while the second term is the co-operative term. In this case both terms have a linear dependence on $1-c$ at small $1-c$. We find that this linear behavior is valid over a surprisingly broad regime, as is evident from Fig. 8(a). In three dimensions, we find that

$$\frac{N}{L^2} \approx 1 + a_1(1-c) + a_2[c(1-c)]^{1/2} e^{-b_0 c/(1-c)}, \tag{37}$$

where a_1, a_2, b_0 are nonuniversal constants. The close fit of this form to the data is evident in Fig. 8(b).

Finally, the energy is related to the number of bonds on the manifold and the weak fraction through the relation

$$E = f_w N \epsilon + (1 - f_w) N. \tag{38}$$

This is an exact equation valid for all c and ϵ. In fact, we use this equation as a check on the consistency of our numerical procedures for calculating f_w, N, and E. Analytic expressions for the energy as a function of c at small $1-c$ are found by combining Eq. (38) with Eqs. (33) and (36) for two dimensions or with Eqs. (34) and (37) for three dimensions. As a

final empirical remark, it is interesting to note that the two dimensional energy data are well described by the simple relation

$$\frac{E}{L} \approx 0.97 - 1.74(1-c) \tag{39}$$

for a broad range of values of $1-c$. We do not have an explanation for why the rather complex expression found from Eq. (38) with Eqs. (33) and (36) should reduce to this simple behavior over such a broad range of $1-c$, though of course a term proportional to $1-c$ is expected from Eq. (38).

Although the unbiased fits of the scaling laws to the numerical data are very good, the parameter values found are not precisely determined. That is, the fits are not markedly worse if the parameter values are varied significantly. This is more severe in three dimensions where the data are restricted to small effective lattice sizes. If the grain size is large and the lattice size is large, we expect the finite size effects to be less severe and the correspondence between the scaling laws and the data to improve. It is thus not surprising that the theory is quite precise in two dimensions. It is also important to note that the unbiased fits of the 3D data lead to different values of the key parameter b_0 in the exponential of the critical length [see Eq. (28)]. The unbiased fits lead to the results $b_0=1.48$ from the roughness data (see the caption to Fig. 9), $b_0=0.53$ from the weak fraction data (see the caption to Fig. 7), and $b_0=0.68$ from the data for the number of bonds on the CM (see the caption to Fig. 8). The values for b_0 should be the same, so we also carried out fits to the data where the value of b_0 is chosen to find a best fit which is most consistent with all of the data. The fits are not significantly worse than those presented in Figs. 7–9 for a fixed value of $b_0=1.0\pm0.2$ with the other parameters free. This suggests that multiple data sets are required to extract reliable fitting parameters from the three dimensional numerical data on the sample sizes currently available.

D. Unified form of scaling theory

In the statistical physics analysis of manifolds, the roughness scaling plays a central role. In this context, it is worth noting that it is possible to state all of the above roughness results in a unified form. To do this, define a scaling length

$$R_c = \min(\xi, g r_c) \tag{40}$$

which is the minimum of the percolative correlation length $\xi=g|c-c_{\mathrm{SAP}}|^{-\nu}$ and energy cutoff length $gr_c=g/\epsilon^{1/D_e}$. The smaller of these two lengths cuts off the percolative fluctuations. Using R_c as the lattice spacing in a nodes link and blobs picture leads to the roughness scaling

$$w \propto R_c (L/R_c)^{\zeta} \quad c < c_{\mathrm{SAP}}. \tag{41}$$

In the regime $c > c_{\mathrm{SAP}}$ we need to take into account the effects of the periodic potential, which leads to

$$w \propto R_c (L/L_c')^{\zeta} \quad c > c_{SAP}, \tag{42}$$

where $L_c'=R_c l_c$ and $l_c=L_c/g$ is given by Eqs. (27) and (28). These scaling forms apply for all values of c, provided $L \gg R_c, L_c$.

V. DISCUSSION AND CONCLUSIONS

We have presented an analysis of the properties of grain-boundary networks where a fraction of the grain boundaries c are strong and the complementary fraction $1-c$ is weak. The grain-boundary networks studied in detail here are random, isotropic grain boundary networks, however, the numerical and analytic procedures we used can be adapted to any given grain boundary or interface network.

We found that the percolation of a strongly connected aggregate occurs at $c_{\mathrm{SAP}}^{2D}=0.38\pm0.01$ in two dimensions, and at $c_{\mathrm{SAP}}^{3D}=0.12\pm0.03$ in three dimensions. The fraction of grains in the polycrystalline material which are part of the percolating aggregrate behaves as $\gamma \propto (c-c_{\mathrm{SAP}})^{\beta}$, for $c > c_{\mathrm{SAP}}$ and $c-c_{\mathrm{SAP}}$ small. The onset of percolation of weak grain boundaries occurs at $c_{\mathrm{WBP}}^{2D}=0.38\pm0.01$ in two dimensions and at $c_{\mathrm{WBP}}^{3D}=0.77\pm0.03$ in three dimensions. In two dimensions $c_{\mathrm{SAP}}=c_{\mathrm{WBP}}$. However, in three dimensions $c_{\mathrm{WBP}} \gg c_{\mathrm{SAP}}$, which means that in three dimensions there is a broad range of concentrations $c_{\mathrm{SAP}}^{3D} < c < c_{\mathrm{WBP}}^{3D}$ where a percolating strong aggregate and a percolating cluster of weak boundaries co-exist. This interpenetrating regime is absent in two dimensions and presents some interesting possibilities in the design of materials which require both access to the material interior as well as strong connectivity of the grain structure. In the case of corrosion, it is desirable to restrict access of corrosive agents to the interior of a material. In some important structural materials special (strong) grain boundaries restrict diffusion of corrosive agents while the remaining (random) boundaries allow diffusion of corrosive agents. In that case it is important to produce materials with the fraction of strong grain boundaries in the range $c > c_{\mathrm{WBP}}$. To further quantify the degree to which corrosive agents penetrate in this regime, we defined a percolative order parameter called the penetration depth l_P, which is the linear size of the largest cluster of weak grain boundaries which is connected to the boundary of the sample. This penetration depth diverges on approach to c_{WBP} from above, with the scaling behavior $l_P \propto (c-c_{\mathrm{WBP}})^{-\nu}$. In practical terms l_P diverges rapidly as $c \to c_{\mathrm{WBP}}$ so that for $c > c_{\mathrm{WBP}}$ there is a very significant decrease in the degree to which corrosive agents can penetrate the material.

The critical manifold (CM) in a random network can be found efficiently using the max-flow/min-cut theorem. The critical manifold is the minimum cut and the maximum flow corresponds to the energy or current carrying capacity of the CM, depending on the application. In the case of polycrystalline high temperature superconductors the maximum flow corresponds to the critical current, while in brittle fracture it corresponds to the energy required to break the bonds which lie on the fracture surface. In the study of CM's we are able to introduce an additional parameter, the energy contrast, which is important in applications. The energy contrast ϵ is the ratio between the "strength" of the weak boundaries and the "strength" of the strong boundaries. In the case of structural applications, the strength corresponds to the bonding energy of the GB while in high temperature superconductors it corresponds to the critical current of the grain boundaries. In the structural applications the typical ratio between the

bonding strength of special boundaries, such as $\Sigma 3$ boundaries, and random boundaries is of order $\epsilon \approx 1/5-1/10$, while in high temperature superconductors, the critical current of high angle boundaries is of order a hundred times lower than that of low angle boundaries, so in that application $\epsilon \approx 1/100$.

We presented data for the cases $\epsilon = 0.0001$, 0.01, 0.1. We studied four aspects of CM's in polycrystalline materials with a fraction c of strong grain boundaries: The energy (or critical current) density E/L^{d-1}, the number of bonds on the CM, N/L^{d-1}; the fraction of the CM that consists of weak grain boundaries, f_w; and the roughness of the CM, w. The CM is sensitive to the percolation of a strong aggregate, so critical scaling of the CM properties occurs at $c = c_{\mathrm{SAP}}$, but nothing special happens to the CM scaling at c_{WBP} as is clear from the results found in three dimensions where $c_{\mathrm{SAP}} \ll c_{\mathrm{WBP}}$. [Note, however, that there are "critical paths" (CP's) that are singular at c_{WBP} as will be described elsewhere.] Large scale simulations were carried out for the four properties above in both two dimensions and in three dimensions (see Figs. 6–9). The energy and the fraction of weak bonds on the CM are monotonic functions of the strong boundary concentration (see Figs. 6 and 7) while the number of bonds on the CM and the roughness of the CM exhibit a peak close to the critical threshold, c_{SAP} (see Figs. 8 and 9).

The numerical results are well described by simple scaling relations adapted from existing theories of random manifolds and periodic elastic media. One simple adaption is that in polycrystalline materials we need to define an effective lattice size L/g, where L is the sample size and g is the average grain size. For $c \ll c_{\mathrm{SAP}}$, the theory of random manifolds applies; for $c \sim c_{\mathrm{SAP}}$ critical scaling based on percolation theory provides an adequate theory; while for $c > c_{\mathrm{SAP}}$ the theory of periodic elastic media applies. The latter regime is perhaps the most interesting from both a theoretical and an application standpoint. In that regime, we define a critical length scale L_c, so that cleavage occurs in regions of typical size L_c and that the CM wanders and roughens on length scales L_c. All of the properties we calculated are related to the scaling behavior of L_c, which is well described by simple scaling laws. The critical length L_c diverges as $c \to 1$. It has an algebraic divergence in two dimensions and in the limit $\epsilon \to 0$ we found an explicit expression for this divergence, $L_c \propto gc/(1-c)$. In three dimensions L_c diverges even more rapidly as $c \to 1$ and (in fact it diverges exponentially), and in the limit $\epsilon \to 0$ we find, $L_c \propto g \exp[b_0 c/(1-c)]/[c(1-c)]^{1/2}$ where b_0 is a nonuniversal constant which is of order 1. From the expression for L_c, it is straightforward to develop scaling laws for many of the properties of interest, for example the manifold energy and its roughness [see Eqs. (30) and (31)]. The peaks observed near c_{SAP} in the roughness and in the number of bonds on the CM are strongly rounded by finite values of the energy contrast ϵ. In two dimensions we found that this peak diverges with energy contrast as $\epsilon^{-0.266}$, while in three dimensions we predicted that this peak grows as $\epsilon^{-0.233}$.

From a statistical physics viewpoint the GBE materials present an interesting opportunity to experimentally test the scaling theories of random manifolds and periodic elastic media. Grain-boundary networks can be controlled carefully and the fraction of weak boundaries can also be controlled, so that the scaling laws for many of the properties of interest can be tested as a function of a tunable concentration c and energy ratio ϵ.

From a practical GBE viewpoint there are some interesting trends and possibilities suggested in the results presented here. One observation is evident from the behavior of the energy density presented in Fig. 6 which corresponds to the critical current in polycrystalline high temperature superconductors. It is clear from this figure that there is a roughly linear improvement in the properties of the critical current of high T_c films for all $c > 0.5$ which means that over 50% of the grain boundaries need to be low angle boundaries in isotropic polycrystalline thin films. In the case of bulk materials, there is a roughly linear regime which has an onset at $c \approx 0.3$ and extends to roughly $c \approx 0.65$. It is thus necessary to have at least 30% of grain boundaries in bulk polycrystalline high T_c materials be low angle boundaries to be in this regime. However, efforts to increase the fraction of low angle boundaries beyond about 65% in bulk materials is relatively futile as the improvement in critical current is relatively slow in this regime. A second potentially interesting feature is the peak in N and w at intermediate values of c, for example in materials where roughness and toughness can be correlated. In using the enhancement in N or w for engineering of toughness one has to be aware of the strong rounding for finite ϵ.

Finally, in GBE modeling it is important to realize that there is a fundamental difference between two and three dimensions. In a broad concentration regime in three dimensions a percolating strong aggregate and a percolating cluster of weak boundaries co-exist. In two dimensions these two percolating clusters do not co-exist. In addition, the scaling behavior of cleavage regions in two dimensions is quite different than that of cleavage regions in three dimensions, especially in the important practical regime $c > c_{\mathrm{SAP}}$. This is due to the fact that L_c diverges algebraically in two dimensions while it diverges exponentially in three dimensions.

ACKNOWLEDGMENTS

The research at MSU has been supported by the DOE under Contract No. DE_FG02-90ER45418, and by Sandia National Laboratories. This work was performed in part at Sandia National Laboratories, a multiprogram laboratory operated by Sandia Corporation, a Lockheed Martin Company, for the United States Department of Energy under Contract No. DE-AC04-94AL85000.

[1] J. Don and S. Majumdar, Acta Metall. **34**, 961 (1986).
[2] D. B. Wells, J. Stewart, A. W. Herbert, P. M. Scott, and D. E. Williams, Corrosion (Houston) **45**, 649 (1989).
[3] L. C. Lim and T. Watanabe, Acta Metall. Mater. **38**, 2507 (1990).
[4] G. Palumbo, P. J. King, K. T. Aust, U. Erb, and P. C. Lichtenberger, Scr. Metall. Mater. **25**, 1775 (1991).
[5] D. C. Crawford and G. S. Was, Metall. Trans. A **23**, 1195 (1992).
[6] K. T. Aust, U. Erb, and G. Palumbo, Mater. Sci. Eng., A **176**, 329 (1994).
[7] T. Watanabe, Mater. Sci. Eng., A **176**, 39 (1994).
[8] Y. Pan, T. Olson, and B. L. Adams, Can. Metall. Q. **34**, 147 (1995).
[9] V. Y. Gertsman, M. Janecek, and K. Tangri, Acta Mater. **44**, 2869 (1996).
[10] V. Y. Gertsman and K. Tangri, Acta Mater. **45**, 4107 (1997).
[11] E. M. Lehockey, G. Palumbo, P. Lin, and A. Brennenstuhl, Metall. Mater. Trans. A **29**, 387 (1998).
[12] G. Palumbo, E. M. Lehockey, and P. Lin, JOM **50**, 40 (1998).
[13] V. Randle, Acta Mater. **47**, 4187 (1999).
[14] T. Watanabe and S. Tsurekawa, Acta Mater. **47**, 4171 (1999).
[15] M. Kumar, W. E. King, and A. J. Schwartz, Acta Mater. **48**, 2081 (2000).
[16] V. Y. Gertsman and S. M. Bruemmer, Acta Mater. **49**, 1589 (2001).
[17] R. W. Minich, C. A. Schuh, and M. Kumar, Phys. Rev. B **66**, 52101 (2002).
[18] C. A. Schuh, M. Kumar, and W. E. King, Acta Mater. **51**, 687 (2003).
[19] D. Dimos, P. Chaudhari, J. Mannhart, and F. K. LeGoues, Phys. Rev. Lett. **61**, 219 (1988).
[20] J. Rhyner and G. Blatter, Phys. Rev. B **40**, R829 (1989).
[21] R. Riedinger, Cryogenics **30**, 464 (1990).
[22] C. S. Nichols and D. R. Clarke, Acta Metall. Mater. **39**, 995 (1991).
[23] M. Prester, Phys. Rev. B **54**, 606 (2002).
[24] E. D. Specht, A. Goyal, and D. M. Kroeger, Phys. Rev. B **53**, 3585 (1996).
[25] R. Haslinger and R. Joynt, Phys. Rev. B **61**, 4206 (2000).
[26] J. L. Reeves, D. M. Feldmann, C. Y. Yang, and D. C. Larbalestier, IEEE Trans. Appl. Supercond. **11**, 3863 (2001).
[27] B. Zeimetz, N. A. Rutter, B. A. Glowacki, and J. E. Evetts, Supercond. Sci. Technol. **14**, 672 (2001).
[28] Y. Nakamura, T. Izumi, and Y. Shiohara, Physica C **371**, 275 (2002).
[29] B. Zeimetz, B. A. Glowacki, and J. E. Evetts, Eur. Phys. J. B **29**, 359 (2002).
[30] B. Zeimetz, B. A. Glowacki, and J. E. Evetts, Physica C **372-376**, 767 (2002).
[31] M. Eisterer, M. Zehetmayer, and H. W. Weber, Phys. Rev. Lett. **90**, 247002 (2003).
[32] M. Frary and C. A. Schuh, Appl. Phys. Lett. **83**, 3755 (2003).
[33] K. Ogawa and K. Osamura, Phys. Rev. B **67**, 184509 (2003).
[34] C. A. Schuh, R. W. Minich, and M. Kumar, Philos. Mag. **83**, 711 (2003).
[35] M. Bartkowiak, G. D. Mahan, F. A. Modine, M. A. Alim, R. Lauf, and A. McMillan, J. Appl. Phys. **80**, 6516 (1996).
[36] D. R. Clarke, J. Am. Ceram. Soc. **82**, 485 (1999).
[37] M. P. Anderson, D. J. Srolovitz, G. S. Grest, and P. Shani, Acta Metall. **32**, 783 (1984).
[38] D. J. Srolovitz, M. P. Anderson, P. S. Sahni, and G. S. Grest, Acta Metall. **32**, 793 (1984).
[39] M. Miodownik, A. W. Godfrey, E. A. Holm, and D. A. Hughes, Acta Mater. **47**, 2661 (1999).
[40] E. A. Holm and C. C. Battaile, JOM **53**, 20 (2001).
[41] G. Deutscher, O. Entin-Wohlman, S. Fishman, and Y. Shapira, Phys. Rev. B **21**, 5041 (1980).
[42] O. Entin-Wohlman, A. Kapitulnik, S. Alexander, and G. Deutscher, Phys. Rev. B **30**, 2617 (1984).
[43] S. Roux, A. Hansen, and E. Guyon, J. Phys. (Paris) **48**, 2125 (1987).
[44] M. Octavio, A. Octavio, J. Aponte, R. Medina, and C. J. Lobb, Phys. Rev. B **37**, 9292 (1988).
[45] E. L. Hinrichsen, S. Roux, and A. Hansen, Physica C **167**, 433 (1990).
[46] D. Stauffer and A. Aharony, *Introduction to Percolation Theory* (Taylor & Francis, London, 1994).
[47] A. Donev, C. E. Musolff, and P. M. Duxbury, J. Phys. A **35**, L1 (2002).
[48] D. A. Huse and C. L. Henley, Phys. Rev. Lett. **54**, 2708 (1985).
[49] V. I. Raisanen, E. T. Seppälä, M. J. Alava, and P. M. Duxbury, Phys. Rev. Lett. **80**, 329 (1998).
[50] J. H. Meinke, E. S. McGarrity, P. M. Duxbury, and E. A. Holm, Phys. Rev. E **68**, 066107 (2003).
[51] A. A. Middleton, Phys. Rev. E **52**, R3337 (1995).
[52] M. J. Alava and P. M. Duxbury, Phys. Rev. B **54**, 14990 (1996).
[53] E. A. Holm, J. Am. Ceram. Soc. **81**, 455 (1998).
[54] E. A. Holm and G. N. McGovney, in *Fracture and Deductive vs. Brittle Behavior—Theory, Modeling and Experiment*, edited by G. E. Beltz, R. L. Lumberg Selinger, M. P. Marder, and K.-S. Kim, Mater. Res. Soc. Symp. Proc. No. 539 (Materials Research Society, Pittsburgh, 1999), p. 325.
[55] J. P. Bouchaud and A. Georges, Phys. Rev. Lett. **68**, 3908 (1992).
[56] T. Emig and T. Nattermann, Eur. Phys. J. B **8**, 525 (1999).
[57] E. T. Seppälä, M. J. Alava, and P. M. Duxbury, Phys. Rev. E **63**, 036126 (2001).
[58] G. S. Was, V. Thaveeprungsriporn, and D. C. Crawford, JOM **50**, 44 (1998).
[59] B. B. Mandelbrot, D. E. Passoja, and A. J. Paulley, Nature (London) **308**, 721 (1984).
[60] T. Engøy, K. J. Måløy, A. Hansen, and S. Roux, Phys. Rev. Lett. **73**, 834 (1994).
[61] E. Bouchaud, J. Phys.: Condens. Matter **9**, 4319 (1997).
[62] E. Bouchaud, J. P. Bouchaud, D. S. Fisher, S. Ramanathan, and J. R. Rice, J. Mech. Phys. Solids **50**, 1703 (2002).
[63] S. Morel, E. Bouchaud, J. Schmittbuhl, and G. Valentin, Int. J. Fract. **114**, 307 (2002).
[64] A. V. Goldberg and R. E. Tarjan, *Proceedings of the eighteenth annual ACM Symposium on the Theory of Computing*, Berkeley, CA, May 28–30, 1986 (ACM Press, New York, 1986), p. 136.
[65] M. J. Alava, P. M. Duxbury, C. F. Moukarzel, and H. Rieger, in *Phase Transistions and Critical Phenomena*, edited by C. Domb and J. Lebowitz (Academic, New York, 2001), Vol. 18.
[66] D. S. Fisher, Phys. Rev. Lett. **56**, 1964 (1986).
[67] P. M. Duxbury, P. L. Leath, and P. D. Beale, Phys. Rev. B **36**, 367 (1987).